vascularity, vascular hyperplasia, nuclear shape, nuclear chromatin, pleomorphism, necrosis, mitosis, apoptosis, and Rosenthal fibers.

Results: There was concordance between smear and final neuropathologic diagnosis regarding both lineage and grade by WHO classification in 25/33 (75%) diffuse gliomas, and the closely mimicking pilocytic astrocytomas (PA). When compared with the final neuropathologic diagnosis, six glioblastoma, 5/10 anaplastic astrocytomas (AA), and one anaplastic oligoastrocytoma (AOA) were correctly classified and graded. Of grade II tumors, 5 astrocytomas (A), 3/4 oligodendrogliomas (O), 2 oligoastrocytomas (OA), and 4/5 PA, including one high-grade were correctly classified. Discrepant cases are described in Tables I and II.

Table I: Gliomas showing discrepancy in WHO grade

Cases	Smear Diagnosis	Final neuropathologic Diagnosis	Discrepancy	Technical reason	Interpretational reason
1	A (grade II)	PA	Minor	1.Thick smear 2. Sampling – absence of Rosenthal fibers	
2	A (grade II)	AA (grade III)	Major	1. Sampling 2. Sparse cellularity	
3	A (grade II)	AA (grade III)	Major	1. Sampling 2. Sparse cellularity	
4	AA (grade III)	PA	Major	1.Thick smears 2. Blood and eosin stain deposits	1. Cellularity, atypia and smudgy chromatin of protoplasmic astrocytes 2. Vascular hyperplasia; in PA.

Table II: Gliomas showing discrepancy in lineage classification

Cases	Smear diagnosis	Final neuropathologic diagnosis	Discrepancy	Technical reasons	Interpretational reasons
1	OA	O	Minor	Smear-induced cell spindling	Deletion of 1p, 19q by FISH
2	AO	AA	Major	Scant tumor	Small cell astrocytoma; 30% p53+; no FISH
3	AOA	AA	Minor		90% p53+; Retained 1p, 19q
4	AOA	AA	Minor		50% p53+; Retained 1p, 19q

Conclusions: There was a high concordance between smear and final neuropathologic diagnosis in diffuse gliomas. Smear analysis is not only complementary to frozen section in the immediate surgical management of gliomas, but is also a reasonable stand-alone diagnostic test, given correct understanding of its capability and limitations.

1702 Pediatric Infratentorial Glioblastomas with Distinct Genotype on FFPE Based aCGH

S Sharma, A Free, Y Mei, SC Peiper, Z Wang, J Cowell. Medical College of Georgia, Augusta, GA; Jefferson Medical College, Philadelphia, PA.

Background: Glioblastomas (GBM) are rare in children, but reportedly have more varied outcome and suggested differences in tumor biology as compared to typical GBM of adults. We performed high resolution array Comparative Genomic Hybridization (aCGH) aiming to identify genomic copy number changes that might define pediatric infratentorial glioblastoma.

Design: Three pediatric infratentorial GBM, ages 3.5, 7 and 14 years were identified from pathology records. DNA was extracted from formalin-fixed, paraffin embedded (FFPE) samples, using the WaxFree sample isolation kit (TrimGen), labeled with biotin and hybridized to the Affymetrix 250K Sty 1 Mapping array. Call rate of >75%, for SNPs permitted optimal visualization of chromosome events using Partek Genomics Suite software.

Results: Two tumors occurred in the brainstem and one in spinal cord. While histologically typical, one brainstem tumor showed mainly pleomorphic astrocytic cells, whereas the other brainstem and spinal tumors showed a GFAP positive small cell component. Whole chromosomal gains (#1, # 2) and loss (#20) were seen only in the pleomorphic brainstem GBM, which also showed a high level of segmental genomic copy number changes. Segmental loss involving chromosome 8 was seen in all three tumors (Chr8;133039446-136869494, Chr8;pter-3581577, Chr8;pter-30480019 respectively), whereas loss involving chromosome 16 was seen in only 2 cases with small cell components (Chr16;31827239-qter, Chr16;pter-29754532). Segmental gain of chromosome 7 was shared only between 2 brainstem cases (Chr7;17187166-qter, Chr7;69824947-qter). The spinal GBM showed a relatively stable karyotype with a unique loss of Chr19;32848902-qter. None of the frequent losses, gains and amplifications known to occur in adult GBM were identified.

Conclusions: This FFPE based, high resolution DNA copy number profiling in the examined subset of pediatric infratentorial glioblastomas shows a molecular karyotype that was more characteristic of pediatric embryonal tumors rather than adult GBM.

1703 Differential Expression of STAT-6 and Activated STAT-6 in Primary Central Nervous System Lymphoma and Peripheral Diffuse Large B-Cell Lymphoma

NT Sherwood, JF Silverman, C Pu, K Ru. Allegheny General Hospital, Pittsburgh, PA.

Background: STAT-6 is a protein transcription factor and member of the signal transduction and activator of transcription (STAT) family. These cytoplasmic proteins become phosphorylated and activated by Janus kinase in response to extracellular cytokines. The phosphorylated STAT protein is then transported to the nucleus where it exerts activation of transcription. STAT6 overexpression has been reported in central nervous system (CNS) B-cell lymphoma by DNA microarray studies. Our aim was to explore the expression level of STAT6 and activated STAT6 (pSTAT6) by immunohistochemical studies in CNS B-cell lymphoma and compared to peripheral diffuse large B-cell lymphoma (DLBCL) and investigate STAT6 activation in the tumorigenesis of these two types of lymphomas.

Design: Paraffin embedded surgical specimens including 14 cases of peripheral DLBCL and 8 cases of primary CNS B-cell lymphoma were retrieved from our files. All cases were stained with STAT6 and pSTAT6. The slides were then reviewed, and staining patterns were recorded as negative, partially positive (weak or focal staining), and strongly positive.

Results: Strongly positive staining for both STAT6 and pSTAT6 were seen in 8 of 8 cases (100%) of primary CNS B-cell lymphoma. As expected, staining was cytoplasmic for STAT6 and nuclear for pSTAT6. Only 3 of 14 cases (21%) of DLBCL were strongly and diffusely positive for either stain. There was weak, focal, or partial staining for STAT6 in 2 of 14 (14%) cases and also for pSTAT6 in 6 of 14 (43%) cases of DLBCL.

Conclusions: The STAT6 and pSTAT6 markers were highly sensitive for detecting primary CNS B-cell lymphoma. The staining patterns were strongly and diffusely positive in all cases of primary CNS B-cell lymphoma. Only 3 of 14 cases of DLBCL exhibited this pattern. The remaining cases of DLBCL were either completely negative or exhibited focal, weak, or partial-positive staining. Median survival for DLBCL may be as high as 5 years depending on subtype, whereas the median survival for primary CNS B-cell lymphoma may be as low as 12-18 months. This may reflect differences in their respective tumorigenesis and related to the STAT6 activation pathway. It would be worthwhile to further investigate this phenomenon with a longitudinal study comparing survival in cases of DLBCL that are strongly positive for STAT6 versus those that are negative or only partially positive. Additionally, STAT6 and pSTAT6 may have a role in future targeted therapy for aggressive CNS B-cell.

1704 Expression of Phospho-p38 MAPK and Phospho-p44/42 MAPK in Gliomas and Correlation with Patients' Outcome

V Zolota, Z Kefalopoulou, C Sirinian, A Argyriou, H Kalofonos. University of Patras Medical School, Patras, Greece.

Background: Gliomas are devastating and aggressive human tumors and molecular pathogenesis has been under intense investigation as a part of the effort to develop more effective therapeutic strategies for these tumors. Mitogen-activated protein kinases (MAPK) are widely expressed serine-threonine kinases mediating important regulatory signals in the cell. Activation of MAPK cascades is believed to play a critical role in malignant transformation. This study investigates the role of expression of phospho-p38 and phospho-p44/42 (Erk1/2), two key components of the MAPK signalling pathway, as prognostic indicators in gliomas.

Design: The expression of p-p38 MAPK and p-p44/42 MAPK was evaluated in 62 gliomas using immunohistochemistry on formalin-fixed paraffin-embedded tissue specimens. Grade II astrocytomas were recorded as low-grade gliomas (n = 13, mean age = 47.6 ± 15.5 years, mean overall survival = 46.3 ± 12.1 months). Grade III anaplastic astrocytomas and grade IV glioblastomas were recorded as high-grade gliomas (n=49, mean age = 58.1 ± 12.3 years, mean overall survival = 18.9 ± 14.2 months). Results were expressed as %tumor cells displaying positive nuclear stain.

Results: The table lists the results. Expression of both markers was associated with more aggressive histological features (increased cellularity, nuclear atypia, mitotic activity, gemistocytes). Statistical analysis revealed a) a higher expression of both p-p38 and p-p44/42 in high-grade compared to low-grade gliomas ($p<0.001$) and b) a strong correlation between the two markers ($r = 0.689$, $p < 0.001$). Univariate analysis revealed that p-p44/42 expression was correlated with worse overall survival ($p = 0.007$). However, Cox regression failed to confirm that p-p44/42 constitutes an independent adverse prognostic factor.

Expression levels of p-p38 and p-44/42 in low- and high-grade gliomas.

	Total cases (n=62)	Low-grade (n=13)	High-grade (n=49)
p-p38	32.2 ± 20.9	9.6 ± 7.4[a]	38.2 ± 19.1[a]
p-p44/42	39.2 ± 22.7	19.4 ± 10.5[b]	44.5 ± 22.2[b]
[a, b] < 0.001			

Conclusions: Up-regulation of p-p38 and p-p44/42 in high-grade gliomas suggests that activation of MAPK signalling pathway may contribute to the acquisition of malignant properties and tumor progression in gliomas. The pathophysiological mechanism underlying the distinctive role of MAPK family in malignant transformation in gliomas as well as any putative therapeutic applications should be further investigated.

Ophthalmic

1705 Eye Pathology in Nephrogenic Systemic Fibrosis

JL Abraham, AE Barker-Griffith. SUNY Upstate Medical University, Syracuse, NY.

Background: Nephrogenic Systemic Fibrosis, first described in 2000, is a debilitating cutaneous and systemic fibrosing disorder. The two known associations with NSF include renal dysfunction and exposure to gadolinium-containing contrast agents (GCCA). Ophthalmic interest stems from the appearance of "scleral injection" in all cases reported by Levine et al and scleral plaques seen clinically in young persons with NSF.

Design: We have reported detection by scanning electron microscopy with energy dispersive X-ray spectroscopy (SEM-EDS) of gadolinium in paraffin embedded skin biopsies of NSF tissue in over 60 cases and a few autopsy cases. Only recently have two autopsy cases included the eyes. These are studied by (SEM-EDS) for evidence of gadolinium and scleral plaques.

Results: SEM-EDS show the scleral plaques to be composed entirely of calcium phosphate with no detectable gadolinium in any of these areas. Gadolinium was discovered around and in blood vessels of the choriocapillaris. In addition, the light microscopy of the scleral plaques are very different from the usual Cogan's plaques of aging.

Conclusions: The scleral plaques observed in NSF may be related more to calcium-phosphorous metabolism disturbances of chronic renal failure and hyperparathyroidism than to specific gadolinium toxicity.

1706 Proposed Prognostic Grading System for Uveal Melanoma on Fine Needle Aspiration Based on Cytomorphologic Features

OA Asojo, Z Correa, SN Masineni, JQ Mo, JJ Augsburger, H Yin. University of Cincinnati, Cincinnati, OH; Cincinnati Children's Hospital, Cincinnati, OH; University of Cincinnati Health Center, Cincinnati, OH.

Background: Uveal melanoma is the most common primary ocular malignancy in adults. Currently, most patients are treated by eye-preserving therapy. Fine needle aspiration cytology (FNAC) is an important diagnostic tool, particularly in delineating simulating lesion. A small-scale study demonstrated excellent cytomorphologic correlation between FNAC and enucleation sections. However, no large studies have been published and no cytology grading system has been established. Such a system is useful in guiding or monitoring treatment and predicting outcome. We propose a grading system combining cytomorphologic features to derive a cytologic diagnosis. We further evaluate the association between cytologic diagnosis and clinical prognostic parameters.

Design: A retrospective review was conducted independently by 3 pathologists on eye fine needle aspirates from 62 cases of uveal melanoma. Cytomorphologic parameters were evaluated: cellularity (score 0-2), atypia (score 0-3), dyscohesion (score 0-1), pigmentation (score 0-2), necrosis (score 0-1) and cell morphology (epitheliod vs spindle). Clinical prognostic parameters include age, sex, ciliary body invasion (CB), tumor largest base diameter (LBD) and thickness of tumor. Spearman correlation analysis was performed to ascertain an association between the cytomorphologic grade and clinical parameters.

Results: Seven cytologic diagnosis were established: 1=Not sufficient for diagnosis (QNS), 2=Nevus, 3=Borderline/Indeterminate, 4= Suspicious for melanoma, 5= Melanoma, spindle type, 6= melanoma, mixed type, 7= Melanoma, epitheliod type. Cytologic grade and diagnosis correlates with tumor thickness ($r=0.3556$; $p=0.0046$), cellularity ($r=0.7173$; $p<0.0001$), dyscohesion ($r=0.7522$; $p<0.0001$), atypia ($r=0.6951$; $p<0.0001$), pigment ($r=0.3992$; $p=0.0013$) and necrosis ($r=0.4482$, $p=0.003$). There was no correlation between CB invasion and LBD.

Conclusions: The proposed grading system of FNAC shows a great promise as a cost-effective way to predict biological behavior of uveal melanoma. This grading method is easy to use and reproducible among pathologists. Adding this grading system to the cytology report may help clinicians patient management and predicting survival.

1707 4E-BP1 and eIF4E in Uveal Melanoma Associate with Prognosis

MC Dinares, C Parada, T Moline, P Huguet, R Medel, V Peg, J Hernandez-Losa, S Ramon y Cajal. Hospital Universitari Vall d'Hebron, Barcelona, Spain; Fundació, Institut de Recerca Hospital Universitari Vall d'Hebron, Barcelona, Spain.

Background: During tumor development regulation of cap-dependent translation is critical to determine the rate of growth and the sensitivity to stimulus like hypoxia, low nutrient concentration and others. This mechanism is tightly controlled by the assembly of the multiprotein complex eIF4F, encompassing among the others eIF4E and eIF4G. eIF4E is sequestered in the cytoplasm by 4E-BP1 and in the nucleus by PML, in both cases rendering eIF4E non-functional. 4E-BP1 is regulated itself by several phosphorylations, controlled by the mTORC1 complex. In this regard, 4E-BP1 has been demonstrating to correlate with poor prognosis and high pathologic rate breast, ovarian and recently in skin melanoma metastasis. The aim of this work is to study the role of these centre of funnel factor in cell signaling in uveal melanoma tumors in order to prove if there is an association with poor prognosis.

Design: Thirty-nine uveal melanomas from enucleated eyes were selected. Immunohistochemistry was performed for 4E-BP1, p4E-BP1, eIF4E, peIF4G, PML and Ki-67.These factors correlated with prognosis and histopathological features of the tumors including size, necrosis and subtype.

Results: From a biological and molecular point of view, a correlation between 4E-BP1 and p4E-BP1 (R2=0,23) was found, as well as p4E-BP1 and eIF4E (R2=0,24) and peIF4G (R2=0,12). Moreover a correlation between p4E-BP1, eIF4E, peIF4G and Ki-67 was detected (R2=0,03; R2=0,01; R2=0,02). Regarding histopathology features, 4E-BP1 expression was associated with intense vascular pattern, p4E-BP1 with larger size (R2=0,06), eIF4E and necrosis and finally Ki-67 with necrosis and also metastasis.

Conclusions: In this study we have observed several correlations between the level of expression of 4E-BP1, p4E-BP1 and eIF4E with size of the tumor, angiogenesis and prognosis. Further studies with a higher number of cases is ongoing to confirm this data.

1708 Non-Hereditary Corneal Amyloid Deposition: A Case Series

JJ O'Brien, ME McLaughlin, N Laver. Tufts Medical Center, Boston, MA.

Background: Corneal amyloid deposition can occur with localized eye disease. Amyloid has been associated with trauma, retinopathy of prematurity, trachoma and phlyctenular disease. A primary localized form of amyloid deposition, polymorphic amyloid degeneration, is a rare, bilateral, non-familial, sporadic disorder of the corneal stroma that is seen in people older than 50 years of age. Clinical findings of this particular disease include punctuate and filamentous, glass-like clear irregularly shaped corneal opacities in the middle and deep stromal layers that are refractile on retroillumination and do not form a distinct lattice pattern. Many corneal dystrophies are a result of mutations in the Transforming Growth Factor Beta Induced (TGFBI) gene that encodes for the BIGH3 protein (keratoepithelin), including lattice corneal dystrophies as well as autosomal dominant polymorphic corneal amyloidosis. AD polymorphic amyloid degeneration is caused by an A546D mutation in the TGFBI gene. Because of the genetic basis, corneal dystrophies are more likely to recur in grafts following corneal transplantation than other corneal disorders. In this series, we review cases of corneas with amyloid deposition without a clinical history suggestive of amyloid degeneration or lattice dystrophy. In these cases, the amyloid deposition is a localized eye disease seen in association with a previous surgery history, or scarring.

Design: Formalin-fixed, paraffin-embedded tissue sections were stained with hematoxylin-eosin, congo red, PAS, alcian blue, and Masson's trichrome in each case. Clinical history and histology were reviewed.

Results: Histological examination revealed corneal scarring, stromal edema, endothelial degeneration, mid-to-deep stromal small, scattered, fusiform, amorphous, eosinophilic deposits. The accumulations were congo-red positive and showed dichroic apple green birefringence, consistent with amyloid deposits. Masson trichrome and alcian blue stains were negative. Four cases were positive for amyloid deposits without a previous clinical history suggestive of lattice dystrophy. The 4 cases were submitted as corneal scarring, corneal edema, bilateral guttata suggestive of Fleck's dystrophy, and penetrating keratoplasty status-post extracapsular cataract extraction and posterior chamber intraocular lens implantation.

Conclusions: Corneas are frequently submitted for a variety of reasons, including graft failure, corneal scarring, and corneal edema. Because the hereditary corneal dystrophies tend to recur in corneal transplants, it is important to evaluate deposits incidentally identified in corneas.

1709 The Role of Flow Cytometry in the Diagnosis of Intraocular Lymphoma

H Olteanu, AM Harrington, SH Kroft. Medical College of Wisconsin, Milwaukee, WI.

Background: Intraocular lymphoma (IOL) is a difficult diagnosis to establish, particularly due to its ability to mimic other ophthalmologic conditions and the limited material available for examination. Patients (pts) with vitritis of unknown cause usually undergo a diagnostic vitrectomy for a suspected intraocular infection or malignancy. For IOL, cytology is often cited as the "gold standard", although adjunct techniques, such as flow cytometry, molecular studies, and cytokine measurement, are also used. We report our findings in a series of pts with vitritis of unknown etiology.

Design: 11 consecutive pts (14 eyes) with posterior segment inflammation underwent pars plana vitrectomy for diagnostic purposes. All samples underwent morphologic and flow cytometry (FC) evaluation, and 8/11 also had PCR for EBV, HSV, VZV, CMV, and Toxoplasma. Four-color FC was performed with an antibody panel including, at a minimum, CD5, CD19, kappa and lambda. Clinical data were available from chart review.

Results: The pts consisted of 4 men and 7 women, mean age of 59 years (range, 14-82), and a median follow-up of 12 months (11-38). 3 pts had a history of diffuse large B-cell lymphoma (DLBCL) involving the CNS, calf, and maxillary sinus, respectively; 2 had prior acute lymphoblastic leukemia; and 1 had chronic lymphocytic leukemia/small lymphocytic lymphoma. 2 pts had a history of kidney transplant and 1 a prior allogeneic stem cell transplant. FC in 4/11 (36%) pts demonstrated the presence of a light-chain restricted B-cell population with high forward light scatter, consistent with large B-cell lymphoma. Of these, 2 had prior DLBCL (CNS and calf), and one was a kidney transplant patient. EBV(+) PCR was + in this last patient, and the eye was the only clinical site of involvement. All patients with FC findings of DLBCL had atypical cells on cytologic examination, although a definite diagnosis of lymphoma was not rendered on a morphologic basis alone. In the 7 patients with negative FC, PCR was CMV(+) in 2 patients and HSV(+) in 1 patient. The remaining patients did not have any positive diagnostic findings, including 1 with a negative conjunctival biopsy.

Conclusions: Our study shows that FC is an effective method for diagnosing IOL. Although follow-up was limited, none of the patients with negative FC developed lymphoma. Interestingly, one of the IOL DLBCLs occurred in a kidney transplant patient with + EBV by PCR, thus qualifying as a post-transplant lymphoproliferative disorder (PTLD). There are few case reports of isolated IOL PTLDs, mostly occurring in pediatric patients.

1710 Angiosarcoma of the Eyelid: A Clinicopathologic Comparison between Isolated Unilateral Eyelid Tumors and Tumors Demonstrating Extra-Palpebral Involvement

JA Papalas, CK Manavi, OP Sangueza, TJ Cummings. Duke University Medical Center, Durham, NC; Wake Forest University School of Medicine, Winston-Salem, NC.

Background: Angiosarcomas of the head and neck tend to involve numerous anatomical structures with an overall dismal prognosis. Reports of primary isolated eyelid involvement are rare.

Design: We report 4 cases of angiosarcoma involving the eyelid as either an isolated tumor or as part of a more diffuse malignant process and compare the features of these two tumor types to cases described in the literature.

Results: Overall average age at which patients develop angiosarcoma involving the eyelid was 72. Patients with isolated tumors most often presented complaining of a discrete mass clinically resembling a stye. Patients with isolated eyelid involvement had better survival with no patients dying (average followup 1.5 years) compared to patients with more diffuse disease. When comparing our patients to those reported in the literature, isolated eyelid involvement arises rapidly, with an average tumor size of 2.08 cm. 25% of tumors are misdiagnosed. No patients develop metastasis and 100% are alive after an average period of 3.2 years. With optimal management, tumor progression after treatment is rare. Patients who have eyelid angiosarcoma with extra-palpebral involvement have tumors ranging between 5-10 cm. 21% of patients develop metastasis. Regardless of the treatment, 68% of these patients develop disease progression and 43% were dead after 3.3 years.

Clinicopathologic comparison of patients with angiosarcoma involving just the eyelid versus patients with tumors involving the eyelid and other structures

	Eyelid	Eyelid and other structures	Wilson-Jones Angiosarcoma (Holden 1987)
number of patients	12	28	74
presentation	rapid	varriable	scalp/face
clinical	50% nodular	varriable	bruise-like macule
ulceration	0%	rarely	14%
misdiagnosed	25%	rarely	rarely
metastasis	0%	21%	23%
survival	100% at 3.2 years	43% dead at 3.3 years	50% died in 15 months
regression	1/16	0%	1/72
treatment	excision	68% surgery, 32% non-surgical	radiation
progression	rare	68%	frequent
Size	2.08 cm	5.0 cm	varriable

Conclusions: Patients with isolated eyelid angiosarcoma present at similar ages to patients with more extensive disease, their tumors rarely progress outward to involve extra-palpebral structures, and they do better with more conservative surgical-oncogical management when compared to patients with eyelid involvement secondary to more extensive face disease.

1711 Systemic IgG4 Disease and Orbital Inflammatory Lesions Including Necrobiotic Xanthogranuloma

K Singh, CG Eberhart. Brown University, Providence, RI; Johns Hopkins Hospital, Baltimore, MD.

Background: IgG4 disease is characterized by mass-forming lesions due to lymphoplasmacytic infiltrates rich in IgG4+ plasma cells with associated sclerosis and a raised serum IgG4 level. Systemic IgG4 disease related orbital inflammatory lesions are rare and poorly understood. We recently encountered a case of orbital necrobiotic xanthogranuloma(NXG) associated with confirmed systemic IgG4 disease. We analyzed the number of IgG4-positive plasma cells in this and an additional 16 orbital inflammatory lesions.

Design: Immunohistochemistry for IgG (polyclonal rabbit anti-human IGG, DAKO) and IgG4 (monoclonal mouse anti-human IGG4, ZYMED laboratories) was performed on formalin fixed, paraffin-embedded sections using standard techniques. IgG and IgG4 positive plasma cells were counted in random (maximum ten) high power fields (40X objective with 10X eyepiece).

Results: The table below summarizes our results for the 17 cases included in the study. The NXG(Figure1) in the confirmed case of systemic IgG4 disease had 119 IgG4 positive plasma cell per HPF (range 83 to 170) with a 55% mean percentage of IgG4 positive plasma cells (range 30% to 84%). The IgG4 positive plasma cell percentages in all other orbital inflammatory lesions were low and only one case of non-specific chronic dacryoadenitis with some sclerosis had 33 % IgG4 positive plasma cells in a single focus.

Diagnosis	Age(range)	M:F	IgG4+ plasma cells/HPF(mean, range)	IgG+ plasma cells /HPF(mean , range)	IgG4/IgG Plasma cell %(mean , range)
Necrobiotic xanthogranuloma(n=2)	62-67	1:1	63(0-170)	191(82-367)	30(0-84)
Chronic non-specific dacryoadenitis(n=10)	15-62	1:4	3(0-50)	56(1-241)	3(0-33)
Pseudotumor(n=4)	12-75	1:3	1(0-11)	35(9-112)	1(0-8)
Fungal infection(n=1)	80	F	1(0-4)	61(26-85)	2(0-5)

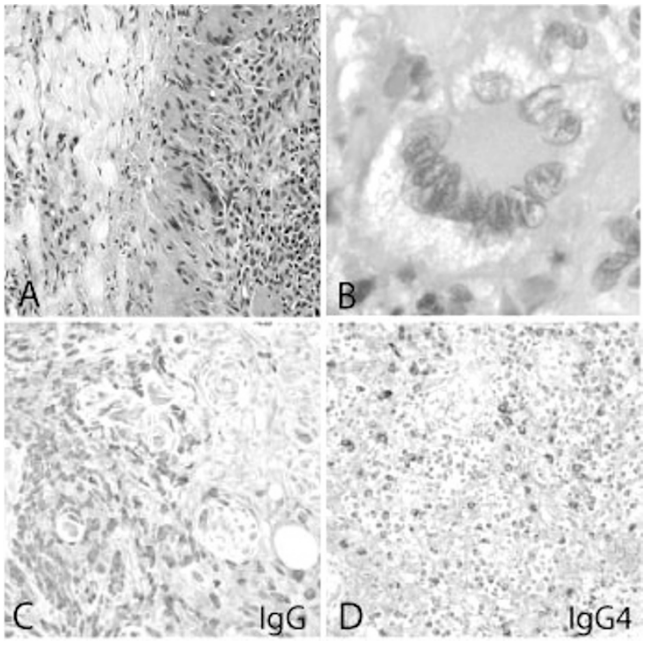

Conclusions: The chronic orbital inflammation cases we analyzed lacking sclerosis or a clear association to systemic IgG4 disease did not show an increase in IgG4 posiitve plasma cells. We conclude that IgG4-positive plasma cell percentages over 30% are uncommon in most orbital inflammatory lesions. We also extend the range of orbital lesions associated with systemic IgG4 disease to include NXG.

1712 Expression of c-KIT by Cell Morphology in Uveal Melanomas

P Tranchida, H Budev, S Sethi, H Jaratli, W Sakr, T Giorgadze. Wayne State University, Detroit, MI.

Background: Uveal melanoma (UM) is the most common primary intraocular cancer in adults. The overall prognosis is unfavorable, with 40-50% of patients developing metastases within 10 years of diagnosis. Recent reports showed that tyrosine kinase inhibitors (TKI) reduce growth in UM-derived cell lines and may be useful in treatment of patients with UM. However, data regarding c-KIT (tyrosine kinase receptor) expression in UM are rare and inconsistent. Our objective was to determine c-KIT immunohistochemical (IHC) expression in UM and correlate the staining patterns with tumor cell types according to modified Callender's classification.

Design: 21 consecutive UM cases treated by enucleation were retrieved (9 females, 12 males; age range: 33-83 years). Immunostaining for c-KIT was performed in representative tissue sections. The staining (cytoplasmic or membranous) was evaluated as negative (<10%), weak (10-50%), or strong (>50%).

Results: The table shows that c-KIT immunoreactivity correlated strongly with the cellular composition of UM. Strong IHC staining was prevalent in spindle cells (both A and B types) and in the spindle cell component of the mixed spindle and epithelioid morphology. Negative or weak IHC expression was evident in all cases of epithelioid UM and the epithelioid component of tumors with mixed morphology. Furthermore, c-KIT staining helped unveil areas with epithelioid morphology in the original H&E sections.

Results of c-KIT immunostaining

Case number	Tumor composition	c-KIT staining (spindle cell)	c-KIT staining (epithelioid)
1	mixed (SB>E)	strong	negative
2	SB	strong	NA
3	SB>SA	strong	NA
4	mixed (SB>SA>E)	strong	negative
5	SA>SB	strong	NA
6	SB	weak	NA
7	mixed (E>SB)	weak	weak
8	SB>SA	strong	NA
9	mixed (E>SB)	strong	negative
10	mixed (E>SB)	weak	negative
11	SB>SA	strong	NA
12	SB	strong	NA
13	mixed (SB>E)	strong	negative
14	SB	strong	NA
15	SB>SA	strong	NA
16	SB	strong	NA
17	mixed (SB>E)	strong	negative
18	SB	negative	NA
19	SB	strong	NA
20	SB	strong	NA
21	E	NA	negative

KEY: E=epithelioid, SA=spindle A, SB=spindle B, NA=Not applicable

Conclusions: Our results show that c-KIT immunoexpression is prevalent in spindle cell UM to the exclusion of purely or predominantly epithelioid tumors. These observations may provide a rationale for considering targeting therapy with TKI only in patients with UM of pure spindle cell type or mixed UM with predominance of spindle cells.

Pathobiology

1713 3'-End Sequencing for Expression Quantification (3SEQ) from Archival Tumor Samples

AH Beck, Z Weng, DM Witten, S Zhu, JW Foley, P Lacroute, CL Smith, R Tibshirani, M van de Rijn, A Sidow, RB West. Stanford University Medical Center, Stanford.

Background: Gene expression microarrays are the most widely used technique for genome-wide expression profiling. However, microarrays do not perform well on formalin fixed paraffin embedded tissue (FFPET). Consequently, microarrays cannot be effectively utilized to perform gene expression profiling on the vast majority of archival tumor samples.

Design: To address this limitation of gene expression microarrays, we designed a novel procedure (3'-end sequencing for expression quantification (3SEQ)) for gene expression profiling from FFPET using next-generation sequencing. We performed gene expression profiling by 3SEQ and microarray on both frozen tissue and FFPET from two soft tissue tumors (desmoid type fibromatosis (DTF) and solitary fibrous tumor (SFT)) (total n = 23).

Results: Analysis of 3SEQ data revealed many genes differentially expressed between the tumor types (FDR < 0.01) on both the frozen tissue (~9.6K genes) and FFPET (~8.1K genes). Analysis of microarray data from frozen tissue revealed fewer differentially expressed genes (4.64K), and analysis of microarray data on FFPET revealed very few (69) differentially expressed genes. Functional gene set analysis of 3SEQ data from both frozen tissue and FFPET identified biological pathways known to be important in DTF and SFT pathogenesis and suggested several additional candidate oncogenic pathways in these tumors.

Conclusions: These findings demonstrate that 3SEQ is an effective technique for gene expression profiling from archival tumor samples and may facilitate significant advances in translational cancer research.

1714 *Trim3*, the Human Homolog of *Drosophila Brain Tumor*, Regulates Neural Differentiation, c-Myc Expression and Glioma Growth Properties

DJ Brat, G Chen, F Rahman, Y Rong, C Tucker-Burden, C Hadjipanayis, EG Van Meir. Emory University School of Medicine, Atlanta, GA.

Background: Glioblastoma (GBM) is the most common malignant brain tumor. A CD133+ stem cell compartment has been described, yet its specialized properties are not